Available online at www.sciencedirect.com
ScienceDirect
Catalysis Today 130 (2008) 462–470
CATALYSIS TODAY
www.elsevier.com/locate/cattod

Modelling and simulation of a gas–solids dispersion flow in a high-flux circulating fluidized bed (HFCFB) riser

J.C.S.C. Bastos [a], L.M. Rosa [a], M. Mori [a,*], F. Marini [a], W.P. Martignoni [b]

[a] *State University of Campinas, Campinas, São Paulo, Brazil*
[b] *PETROBRAS/CENPES, Rio de Janeiro, Brazil*

Available online 3 December 2007

Abstract

Radial solids velocity profiles were computed on seven axial levels in the riser of a high-flux circulating fluidized bed (HFCFB) using a two-phase 3-D computational fluid dynamics model. The computed solids velocities were compared with experimental data on a riser with an internal diameter of 76 mm and a height of 10 m, at a high solids flux of 300 kg m^{-2} s^{-1} and a superficial velocity of 8 m s^{-1}. Several hundreds of experimental and numerical studies on CFBs have been carried out at low fluxes of less than 200 kg m^{-2} s^{-1}, whereas only a few limited useful studies have dealt with high solids flux. The k–ε two-phase turbulence model was used to describe the gas–solids flow in an HFCFB. The model predicts a core–annulus flow in the dilute and developed flow regions similar to that found experimentally, but in the region of highest solids concentration it is somewhat overpredicted at the level close to the inlet.

Keywords: High-flux circulating fluidized bed (HFCFB); k–ε turbulence model; Gas–solids flow

1. Introduction

Two-phase turbulent flows (gas–solids) are involved in many industrial processes such as pneumatic conveyance of particulate materials, gasification, combustion and treatment of environmental pollution. The fast fluidization operation, which occurs under turbulent conditions and has been used since 1942 for the catalytic cracking process, has been responsible for this becoming the most important oil refinery conversion process, indispensable for modern refineries. Catalytic cracking is a chemical process whose goal is to increase the production of gasoline and liquefied petroleum gas (LPG) in refineries, by converting heavy fractions produced by the distillation of oil.

The dynamic behavior of a high-flux gas–solids fluidized bed is defined by the complex interaction between its individual phases. Previous research indicates that this type of flow can be described as having a dense area at the bottom of the riser and a dilute region in its upper section. The radial flow is defined as *core–annulus*, as it has a dilute central solids region with high velocities for both fluid and solids and a high solids concentration near the walls.

In fast fluidization, two different forms of distribution along the riser are usually observed. One of these, where the particulate solids are distributed relatively uniformly along the riser, is shown in Fig. 1(a). In the other, however, there are two completely different phases coexisting in the riser, i.e., a dense phase at the bottom and a dilute phase at the top of the riser, as shown in Fig. 1(b). The circumstances under which these different particulate arrangements occur have not been explained in the literature [8,9].

The nature of the particle distribution – as a continuous dense phase maybe containing bubbles, a continuous gas phase maybe containing clusters or a combination of these – depends on the gas rate. If the gas rate is low, a dense bed will form. However, if the gas rate is high, a dilute system will develop.

At low gas rates with dense bed formation, just a portion of the riser must be fed. An example of this is a system where the riser is high and the pressure drop requirement is low. Solids circulation around the circuit occurs as a result of the solids transition from the dense phase to the dilute phase.

This transition rate decreases with the height of the dense phase surface, and then the spreading of the solids in a dilute

* Corresponding author at: State University of Campinas, Department of Chemical Processes, School of Chemical Engineering, P.O. Box 6066, 13083-970 Campinas, SP, Brazil. Tel.: +55 19 3521 3963; fax: +55 19 3521 3910.
E-mail address: mori@feq.unicamp.br (M. Mori).

0920-5861/$ – see front matter
doi:10.1016/j.cattod.2007.10.075

Nomenclature

C_d	drag coefficient
C_μ, $C_{\varepsilon 1}$, $C_{\varepsilon 2}$, σ_k, σ_ε	constants of the turbulence model
d_p	particle diameter (m)
G	elasticity modulus (Pa)
k	turbulent kinetic energy ($m^2\ s^{-2}$)
P	mean pressure (Pa)
P_k	turbulence production ($m^2\ s^{-3}$)
Re	Reynolds number
S^m	momentum transformation
S^ρ	source term of continuity
U	superficial velocity ($m\ s^{-1}$)
$\vec{v}$	velocity vector ($m\ s^{-1}$)
x, y, z	spatial coordinate (m)

Greek letters

α	volume fraction
β_{gs}^m	momentum transfer coefficient
ε	edge turbulent dissipation ($m^2\ s^{-3}$)
μ	laminar viscosity (Pa s)
μ_t	turbulent viscosity (Pa s)
θ_s	particle sphericity
ρ	density ($kg\ m^3$)

Subscripts

g	related to the gas phase
s	related to the particulate phase

phase occurs. If the gas rate is increased in the system, the dense phase level will increase and the rate of solids transition from the dense phase to the dilute phase will also be at a higher level. This corresponds to the conveying mechanism analyzed and described by He and Rhodes [8] and Rhodes and Geldart [19,20].

In high particulate solids flow (300 $kg\ m^{-2}\ s^{-1}$), Pärssinen and Zhu [18] observed that with the increase in gas superficial velocity, the dense and dilute regions start at lower axial levels, suggesting a faster flow development. However, when the solids flow increases, there is not a significant change in the measured properties of the development at a constant gas velocity. In this experiment, they showed that the particle acceleration (and consequently the development of the flow) departs from the center and extends to the wall. This dictates the development of the radial profiles of particle velocity.

Multiphase flow equations have been developed and analyzed by many researchers, such as He and Rudolph [8], Theologos and Markatos [24] and Ali and Rohani [1]. However, Soo [23] is credited with the mathematical approach to this type of flow. Rietema and van der Akker [21] presented a detailed derivation of the momentum equations for disperse two-phase systems, Michaelides [15] developed a model based on the phenomenological methods for the behavior of the variable density in pneumatic conveying lines and Crowe [6] reviewed the numerical models for dilute gas particle flow.

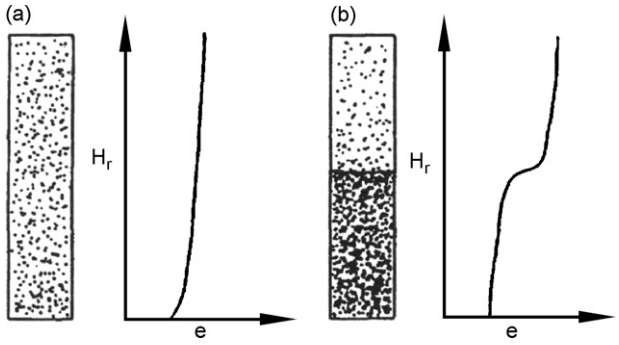

Fig. 1. Two different forms of solids distribution in the riser.

Currently, two of the most well-known methods for the mathematical modelling of the particulate solids phase in numerical simulations of gas–solids flows are the discrete particle simulation and the two-fluid approach. In both approaches the gas phase is described as a local average of the Navier–Stokes equation and both phases are usually connected by a drag force. At first, the dense gas–solids problem could be resolved using just the Newton motion equations for each suspended particle and the Navier–Stokes equation for the gas phase. However, due to the large number of particles, the resultant number of equations would be very large to allow a direct solution, at least with the computer capacity currently available. Thus, the particulate solids phase is also treated as a continuous phase, exposed to the analogous conservation equations for the fluid phase. The Eulerian–Eulerian approach (two fluids approach) proved to be capable of predicting the gas–solids flow, as seen in the research realized by Meier and Mori [12] and Alves et al. [3–5].

In general, the performance of the current models critically depends on the accuracy of the formulation of the drag force, which has been extensively analyzed in many studies on multiphase flows. However, as the drag force follows empirical models, it is of extreme importance that this model be evaluated in accordance with the equipment employed. Gidaspow [7] presented a model for the gas–solids drag correlation, which proved to be sufficiently satisfactory for cyclone flows [14,12] and for riser-type reactors [2,3].

Intending to analyze the physical properties of the gas–solids flow inside risers only along height, several authors, such as Ali and Rohani [1] and Martignoni and de Lasa [11], have presented unidimensional models. These models allowed the simulation up to 500 min and evaluation of the dynamic response of the system. Nieuwland et al. [17] proposed the use of a cylindrical bidimensional geometry, where only one sector of the reactor was calculated. With this model, the same authors were able to get radial profiles, showing the existence of radial segregation. Using a rectangular bidimensional geometry without axial symmetry, Samuelsberg and Hjertager [22] observed the formation of clusters and also noted that the concentration profile followed the standard *core–annulus* profile. In the research of Neri and Gidaspow [16], both Cartesian and cylindrical bidimensional geometries (with and without axial symmetry surfaces) were compared. They observed that the results obtained with Cartesian bidimensional geometry with axial symmetry were similar to

those obtained with cylindrical bidimensional geometry. The effect of turbulence on particle motion in gas–solids suspension was analyzed by Yoshida and Masuda [25], Crowe [6], Alves et al. [3] and Zhang and Reese [26].

2. Mathematical model

The equations used for the gas and particulate solids phases, which are included in the description of the mathematical model, were developed with an Eulerian–Eulerian phenomenological approach, assuming a continuous and interpenetrating representation of the phases that ignores the material discontinuity and its composition (atoms, molecules and particles); in other words, molecular interactions are rejected. Differential equations in the balance are formulated for mass and momentum treating the gas phase as incompressible. According to this approach, different phases can divide the same control volume at the same instant.

The k–ε model was applied to determine the influence of turbulence on the gas phase. Appropriate constitutive equations are specified for the description of the rheological physical properties of each phase and for the closure of the conservation equations.

2.1. Momentum and continuity conservation equations

The momentum and continuity conservation transient equations for each phase (gas and particulate solids) are as follow:

- Continuity equation, gas phase

$$\frac{\partial}{\partial t}(\alpha_g\rho_g) + \frac{\partial}{\partial x}(\alpha_g\rho_g v_{g,x}) + \frac{\partial}{\partial y}(\alpha_g\rho_g v_{g,y}) + \frac{\partial}{\partial z}(\alpha_g\rho_g v_{g,z}) = S_g^{\rho} \tag{1}$$

- Continuity equation, particulate solids phase

$$\frac{\partial}{\partial t}(\alpha_s\rho_s) + \frac{\partial}{\partial x}(\alpha_s\rho_s v_{s,x}) + \frac{\partial}{\partial y}(\alpha_s\rho_s v_{s,y}) + \frac{\partial}{\partial z}(\alpha_s\rho_s v_{s,z}) = S_s^{\rho} \tag{2}$$

where α_g and α_s are the volume fractions; ρ_g and ρ_s are the density of both phases, gas and particulate solids, respectively; $\vec{v}$ is the velocity vector, which can be decomposed into v_x, v_y and v_z; and S_i^{ρ} represents the source term of continuity for each phase.

In the particular case of this research, the mass source terms are null due to the assumption of no mass transfer between phases.

$$S_g^{\rho} = S_s^{\rho} = 0 \tag{3}$$

- Momentum equation, gas phase (x direction)

$$\frac{\partial}{\partial t}(\alpha_g\rho_g v_{g,x}) + \sum_{\xi=x,y,z}\frac{\partial}{\partial\xi}\left(\alpha_g\rho_g v_{g,x}v_{g,\xi} - \alpha_g\mu_g\left(\frac{\partial v_x}{\partial\xi} + \frac{\partial v_\xi}{\partial x}\right)\right) = S_{g,x}^{m} \tag{4}$$

$$S_{g,x}^{m} = \beta_{gs}^{m}(v_{s,x} - v_{g,x}) + \alpha_g\rho_g g_x - \frac{\partial p_g}{\partial x} \tag{5}$$

- Momentum equation, gas phase (y direction)

$$\frac{\partial}{\partial t}(\alpha_g\rho_g v_{g,y}) + \sum_{\xi=x,y,z}\frac{\partial}{\partial\xi}\left(\alpha_g\rho_g v_{g,y}v_{g,\xi} - \alpha_g\mu_g\left(\frac{\partial v_y}{\partial\xi} + \frac{\partial v_\xi}{\partial y}\right)\right) = S_{g,y}^{m} \tag{6}$$

$$S_{g,y}^{m} = \beta_{gs}^{m}(v_{s,y} - v_{g,y}) + \alpha_g\rho_g g_y - \frac{\partial p_g}{\partial y} \tag{7}$$

- Momentum equation, gas phase (z direction)

$$\frac{\partial}{\partial t}(\alpha_g\rho_g v_{g,z}) + \sum_{\xi=x,y,z}\frac{\partial}{\partial\xi}\left(\alpha_g\rho_g v_{g,z}v_{g,\xi} - \alpha_g\mu_g\left(\frac{\partial v_z}{\partial\xi} + \frac{\partial v_\xi}{\partial z}\right)\right) = S_{g,z}^{m} \tag{8}$$

$$S_{g,z}^{m} = \beta_{gs}^{m}(v_{s,z} - v_{g,z}) + \alpha_g\rho_g g_z - \frac{\partial p_g}{\partial z} \tag{9}$$

where μ_g is the viscosity and S_g^{m} represents the momentum transformation of the gas phase.

Analogous equations can be written for the particulate solids phase, considering that the source term expression for pressure force is adjusted with an appropriate expression:

- Momentum equation, particulate solids phase (x direction)

$$\frac{\partial}{\partial t}(\alpha_s\rho_s v_{s,x}) + \sum_{\xi=x,y,z}\frac{\partial}{\partial\xi}\left(\alpha_s\rho_s v_{s,x}v_{s,\xi} - \alpha_s\mu_s\left(\frac{\partial v_x}{\partial\xi} + \frac{\partial v_\xi}{\partial x}\right)\right) = S_{s,x}^{m} \tag{10}$$

$$S_{s,x}^{m} = \beta_{gs}^{m}(v_{g,x} - v_{s,x}) + \alpha_s\rho_s g_x - G\frac{\partial\alpha_s}{\partial x} \tag{11}$$

where the term $G(\partial\alpha_s/\partial x)$ in Eq. (11), coupled to the source term, is a simple model for the solids pressure adjustment (fluidized bed case), which is related to all other spatial directions. G represents the elasticity modulus; the convenient form to express it is given by Eq. (12) [8]:

$$G = G_0\exp[-\kappa(\alpha_s - \alpha_{s,max})] \tag{12}$$

with typical values of $\kappa = 600$, $G_0 = 1.0$ Pa and $\alpha_{s,max} = 0.62$.

- Momentum equation, particulate solids phase (y direction)

$$\frac{\partial}{\partial t}(\alpha_s\rho_s v_{s,y}) + \sum_{\xi=x,y,z}\frac{\partial}{\partial\xi}\left(\alpha_s\rho_s v_{s,y}v_{s,\xi} - \alpha_s\mu_s\left(\frac{\partial v_y}{\partial\xi} + \frac{\partial v_\xi}{\partial y}\right)\right) = S_{s,y}^{m} \tag{13}$$

$$S_{s,y}^{m} = \beta_{gs}^{m}(v_{g,y} - v_{s,y}) + \alpha_s\rho_s g_y - G\frac{\partial\alpha_s}{\partial y} \tag{14}$$

- Momentum equation, particulate solids phase (z direction)

$$\frac{\partial}{\partial t}(\alpha_s\rho_s v_{s,z}) + \sum_{\xi=x,y,z}\frac{\partial}{\partial\xi}\left(\alpha_s\rho_s v_{s,z}v_{s,\xi} - \alpha_s\mu_s\left(\frac{\partial v_z}{\partial\xi} + \frac{\partial v_\xi}{\partial z}\right)\right) = S_{s,z}^{m} \tag{15}$$

$$S_{s,z}^{m} = \beta_{gs}^{m}(v_{g,z} - v_{s,z}) + \alpha_s\rho_s g_z - G\frac{\partial\alpha_s}{\partial z} \tag{16}$$

where S_s^m represents the momentum transformation in the particulate solids phase.

2.2. Turbulence

Turbulence is the elemental key in a rapid particles–fluid mixture flow. It is characterized, according to Reynolds, as the appearance of instabilities in an originally stable flow (the laminar condition), which increase as a nonlinear process and finally develop in a turbulent regime. Due to the fact that fast fluidization operations in riser-type reactors remain under turbulent conditions, the coupling of adequate models to describe the turbulent fluctuation effects is necessary.

The k–ε turbulence model, in which the velocity and length scales are determined with separate transport equations, is used extensively for the determination of gas-phase turbulence because it offers good agreement between numeric effort and computational accuracy. Turbulent kinetic energy k is defined as the variation in velocity fluctuations. The edge turbulent dissipation ε is defined as the rate at which the velocity fluctuations dissipate and it has dimensions of k per time unit.

The exact determination of the effective viscosity of the particulate solids phase is fundamental in attaining the radial distribution of the particles, and consequently, all the fluid dynamics variables [2]. The dispersion models for the particulate solids phase applied to this research were the Newtonian constant transfer coefficient (around 1% higher than gas-phase dynamic viscosity) and null viscosity (inviscid). The effective viscosity is the sum of dynamic viscosity and turbulent viscosity:

$$\mu_{g,ef} = \mu_g + \mu_{g,t} \tag{17}$$

where $\mu_{g,t}$ is the turbulence viscosity.

The model assumes that turbulent viscosity depends on the turbulent kinetic energy and the turbulent kinetic energy dissipation, through the relation proposed by Prandtl and Kolmogorov:

$$\mu_{g,t} = C_\mu \rho_g \frac{k^2}{\varepsilon} \tag{18}$$

where C_μ is a constant of the turbulent model with a value of 0.09.

The values of k and ε are given directly by solution of the differential transport equations for the kinetic energy and turbulent dissipation rate (Eqs. (19) and (20), respectively):

$$\frac{\partial}{\partial t}(\alpha_g \rho_g k) + \nabla \cdot (\alpha_g \rho_g \vec{v}_g k) = \nabla \cdot \left[\left(\mu_g + \frac{\mu_{g,t}}{\sigma_k} \right) \nabla k \right] + P_k - \alpha_g \rho_g \varepsilon \tag{19}$$

$$\frac{\partial}{\partial t}(\alpha_g \rho_g \varepsilon) + \nabla \cdot (\alpha_g \rho_g \vec{v}_g \varepsilon) = \nabla \cdot \left[\left(\mu_g + \frac{\mu_{g,t}}{\sigma_\varepsilon} \right) \nabla \varepsilon \right] + \frac{\varepsilon}{k}(C_{\varepsilon 1} P_k - C_{\varepsilon 2} \alpha_g \rho_g \varepsilon) \tag{20}$$

where $C_{\varepsilon 1}$, $C_{\varepsilon 2}$, σ_k and σ_ε are constants of the k–ε turbulence model with values of 1.44, 1.92, 1.0 and 1.3, respectively. P_k is the production of turbulence due to the viscous forces and buoyancy forces, expressed by

$$P_k = \mu_{g,t} \nabla u_g \cdot (\nabla \vec{v}_g + \nabla \vec{v}_g^T) - \tfrac{2}{3} \nabla \cdot \vec{v}_g (3\mu_{g,t} \nabla \cdot \vec{v}_g + \alpha_g \rho_g k) + P_{kb} \tag{21}$$

2.3. Constitutive equations

2.3.1. Continuity between the phases

$$\sum_i \alpha_i = \alpha_g + \alpha_s = 1 \tag{22}$$

2.3.2. Interphase momentum exchange

The coefficients of friction or drag between fluid and particles are obtained from standard correlations with the negligence of acceleration. Without acceleration, friction on the wall or gravity, the unidimensional momentum balance for the gas phase is

$$\alpha_g \frac{\partial p_g}{\partial x} - \beta_{gs}^m (v_g - v_s) = 0 \tag{23}$$

The momentum transfer coefficient β_{gs}^m is obtained by comparison with Eq. (23), which results in the Ergun equation [10]:

$$\frac{\Delta p}{\Delta x} = 150 \frac{\alpha_s^2 \mu_g U}{\alpha_g^3 (\theta_s d_p^2)} + 1.75 \frac{U^2 \alpha_s \rho_g}{\alpha_g^3 (\theta_s d_p)} \tag{24}$$

where U is the superficial velocity, $U = \alpha_g(v_g - v_s)$, and θ_s is the particle sphericity; in this particular case, $\theta_s = 1$ was used.

The comparison between Eqs. (23) and (24) shows that for dense regimes (with $\alpha_g < 0.8$), the momentum transfer coefficient between gas phase and particles is in accordance with the following equation:

$$\beta_{gs}^m = 150 \frac{\alpha_s^2 \mu_g}{\alpha_g d_p^2} + 1.75 \frac{|v_s - v_g| \alpha_s \rho_g}{d_p} \tag{25}$$

where d_p is the particle diameter of the catalyst.

For porosities higher than 0.8, the expression for pressure drop results in the following equation for the interphase momentum transfer coefficient (Crowe [6]); this was also used in the simulation of Meier and Mori [13]:

$$\beta_{gs}^m = \frac{3}{4} C_d \frac{|v_s - v_g| \alpha_s \rho_g}{d_p} \alpha_g^{-2.65} \tag{26}$$

The Reynolds equation for the particle is given by

$$Re_p = \frac{|v_s - v_g| \rho_g d_p}{\mu_g} \tag{27}$$

The drag coefficient, C_d, applied to Eq. (26), is a function of the Reynolds number and behaves according to (for $Re_p < 1000$)

$$C_d = \alpha_g^{-1.65} \max \left[\frac{24}{Re_p \alpha_g} (1 + 0.15 (Re_p \alpha_g)^{0.687}) \right] \tag{28}$$

Table 1
Solids viscosity used in the simulations

	μ_g (kg m^{-1} s^{-1})	Time (s)
Case 1	0	15
Case 2	1.85×10^{-5}	15
Case 3	1.85×10^{-5}	37

or (for nonlaminar flows, with $Re_p > 1000$)

$$C_d = 0.44 \quad (29)$$

3. Simulation

The simulated model basically consists of a turbulent flow, where two phases enter into contact; a gas phase formed by air at 25 °C with a controlled humidity of 70% and a particulate solids phase composed of catalysts. The particles are considered smooth, spherical and inelastic, with an average diameter of 67 μm and a density of 1500 kg m^{-3}. Table 1 shows three conditions for solids viscosity.

Due to the force of the fluid phase, which achieves the effective weight of particles, these accelerate and move in the flow direction, characterizing the fast fluidized regime in a short space of time along the equipment. In the vertical cylindrical duct (riser), the phases are fed at the base, forming angles of 0° (for the gas-phase entrance) and of 45° (for the particulate solids-phase entrance) in relation to the riser. The exit is located at the top at an angle of 90°, in accordance with Fig. 2.

The measurements were taken at seven axial levels of the equipment, which has a height of 10 m and an internal diameter of 76 mm (z = 1.53 m, 2.73 m, 3.96 m, 5.13 m, 6.34 m, 8.74 m and 9.42 m) and at its respective radial position in accordance with the experimental data of Pärssinen and Zhu [18].

3.1. Boundary conditions

At the entrance, all velocities and concentrations of both phases are specified. The gas-phase pressure, treated as incompressible, was defined at the exit, assuming atmospheric pressure. As initial conditions, the superficial gas velocity is specified as 8 m s^{-1} and the solids flow as 300 kg m^{-2} s^{-1}. At the walls, the gas-phase velocity is zero; the particulate solids-phase velocity has a free-slip condition.

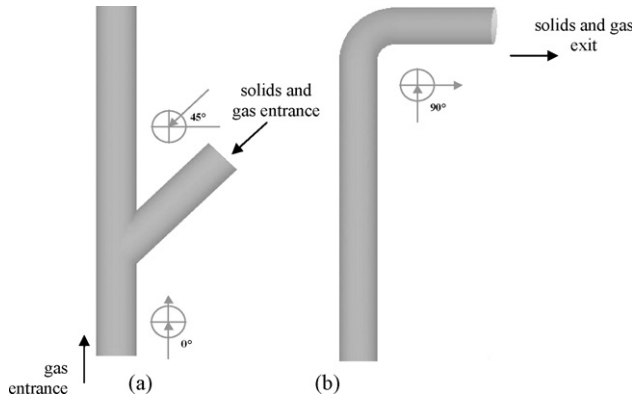

Fig. 2. Entrances (a) and exit (b) of the analyzed riser.

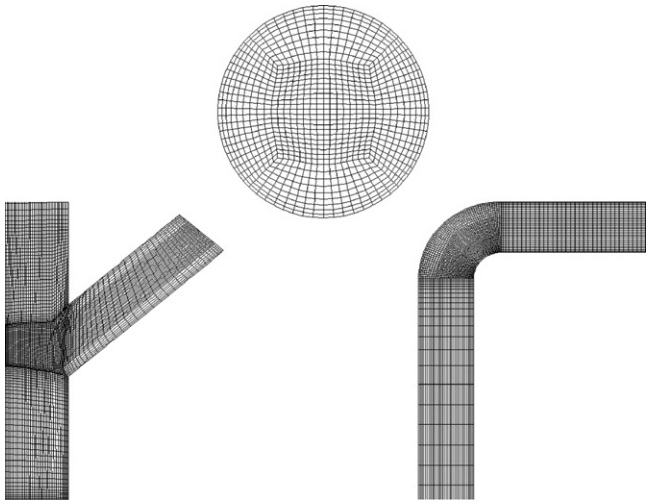

Fig. 3. Numerical mesh details at the entrances and the exit of the equipment.

3.2. Mesh and computational code

The nonstructured mesh is composed of 585,000 control volumes. The details of its refinement, both at the entrances and at the exit, are presented in Fig. 3. The length of the control volumes together near the walls is approximately 1 mm in the radial direction. The time step is on the order of 10^{-3} s. Adaptation of the mathematical model for the numerical model generation was achieved with the use of the ANSYS CFX 10.0 commercial simulator, which is based on the finite volume method, incorporating the higher upwind interpolation scheme.

4. Results and discussion

4.1. Mesh tests

Initially the numerical meshes were tested done and the one that had the best behavior in the standard flow would be used to begin the simulations for the real process. The particle velocity radial profiles for the HFCFB riser were analyzed, using the same conditions as those proposed by Pärssinen and Zhu [18].

In the dependency evaluation of the flow with the numerical mesh, it is known that an adequate number of control volumes is of extreme importance to avoid numerical errors, which is not possible with less refined meshes. Thus, seven meshes, with 234,000, 337,000, 417,000, 470,000, 585,000, 635,000 and 828,000 control volumes, respectively, were tested.

The mathematical model used for numerical mesh simulation was monophase, in accordance with the practice normally adopted, i.e., the flow inside the equipment is purely gaseous, subjected to conservation equations of continuity and momentum for each phase.

The simulations with different meshes resulted in the following observations:

- *Axial dependency* ($r = 0$ m and $z = 0$–10 m): There is not a significant influence on the mesh refinement in the axial direction. However, a slight variation was verified in the less refined mesh in the feed contact region, which is considered a critical point in the equipment.
- *Radial dependency* ($z = 0.3$ m): In this transversal section, practically in the feed contact region, the radial behavior of the flow is analogous to that described for the axial dependency.
- *Radial dependency* ($z = 5.0$ m): In the transversal section at the center of the riser, an insignificant influence of the refined mesh is still observed; all meshes provided the same qualitative profile and quantitative profile.
- *Radial dependency* ($z = 9.5$ m): Dependency on the refined mesh is more noticeable in the exit region, despite the tenuous difference. However, this does not modify the qualitative results.

Then the mesh composed of 585,000 control volumes was chosen; this was shown to be in accordance with the established standards (i.e., there is not a significant difference between the calculated flow of this mesh and those of more refined ones).

4.2. Dispersion model verification

The simulations carried out throughout this research showed that in each one of the transversal sections, there are three distinct zones: a dilute central zone (i.e., a zone where the particle concentration is very low, and consequently its velocity is high, that extends from the radial center ($r = 0$) to approximately $r = 0.02$ m; an intermediate zone with a moderate particle velocity (approximately between $r = 0.02$ m and 0.032 m); and a wall zone with a low particle velocity that extends from approximately $r = 0.032$ m to 0.04 m.

In the axial direction, different regions were also observed: a region of phase contact where the highest solids concentration along the equipment is seen, from the bottom section of the riser extending to a height of approximately 4 m; a middle region with intermediate solids holdups normally observed under low-flux conditions from 4 m to 8 m of height; and a dilute region at the top where the low solids concentration is observed from approximately $h = 8$ m up to the end of the reactor ($h = 10$ m). The fluid dynamics behavior of the HFCFB is similar to that observed under low-flux conditions. However, the solids concentration near the wall region is much higher in the HFCFB than that found under the low-flux conditions.

Different simulations were realized to discover the flow dynamics in terms of the dispersion model used for the solids phase. One of these considered the solids as inviscid and the other considered a constant value of particles viscosity as 1% higher than the gas-phase viscosity. These simulations were carried out until a real time of 15 s was reached. Both simulations showed that the inviscid dispersion model, which considers inviscid particles, has a satisfactory qualitative behavior from the middle region to the top dilute region. However, it does not fit the region of high solids concentration ($h = 0$–4 m).

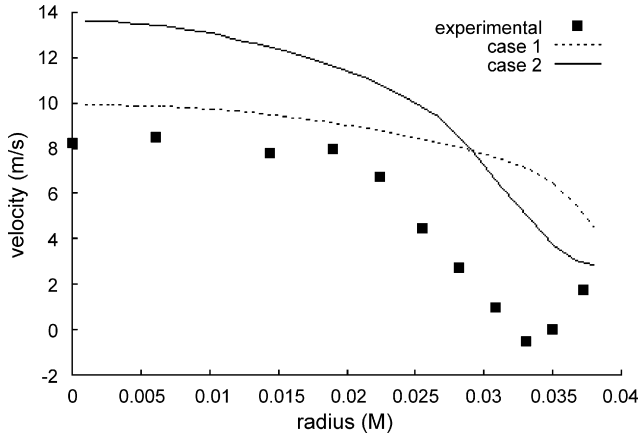

Fig. 4. Profiles of solids velocity at a height of 1.53 m.

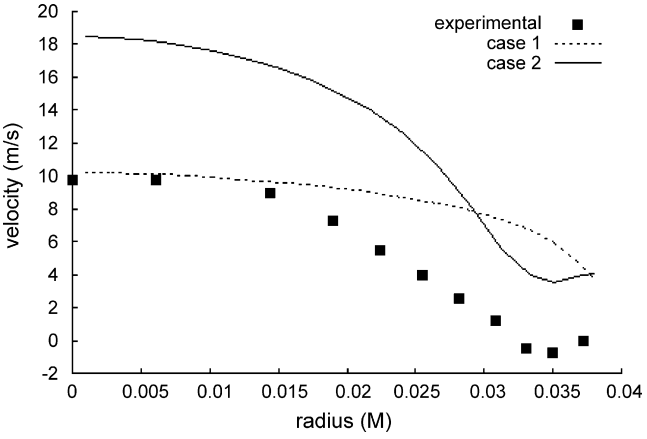

Fig. 5. Profiles of solids velocity at a height of 2.73 m.

Figs. 4 and 5 show the profiles of solids velocity in the dense region ($h = 1.53$ and 2.73) of high solids concentration. It can be observed that the inviscid model has quantitative behavior in the central zone and better results than when used with the constant coefficient Newtonian model (case) 2, but this behavior is inverted closer to the wall.

Figs. 6–8 show the profiles of velocity in the middle flow region at heights of 3.96 m, 5.13 m and 6.34 m, respectively. The computed profiles predict better with experiments in the

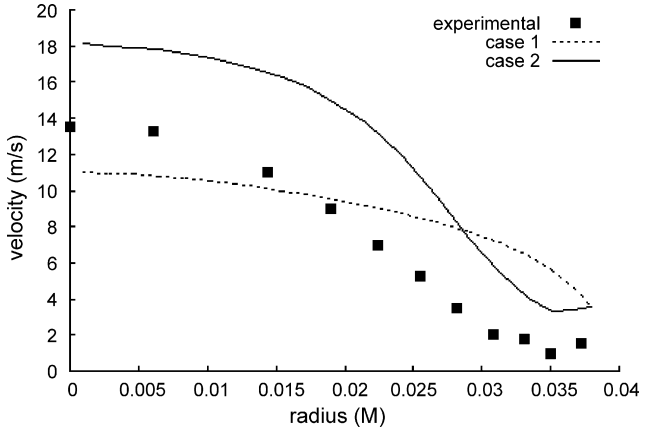

Fig. 6. Profiles of solids velocity at a height of 3.96 m.

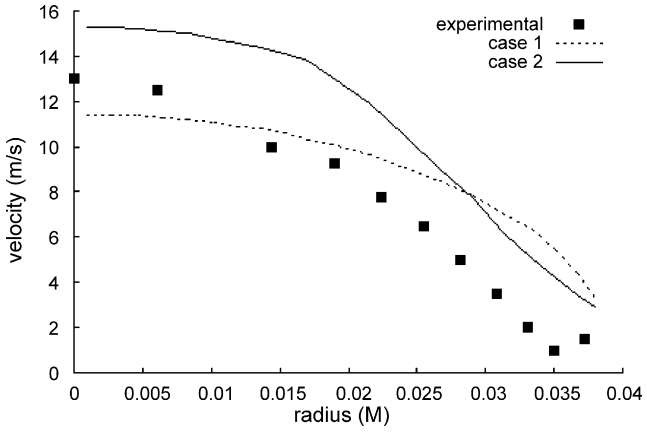

Fig. 7. Particulate solids velocity at a height of 5.13 m.

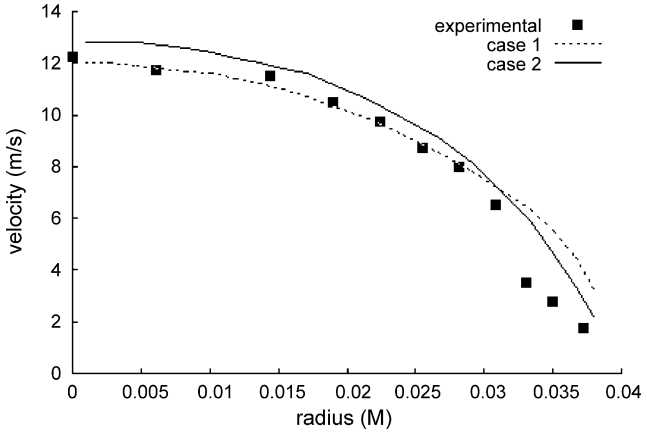

Fig. 8. Profiles of solids velocity at a height of 6.34 m.

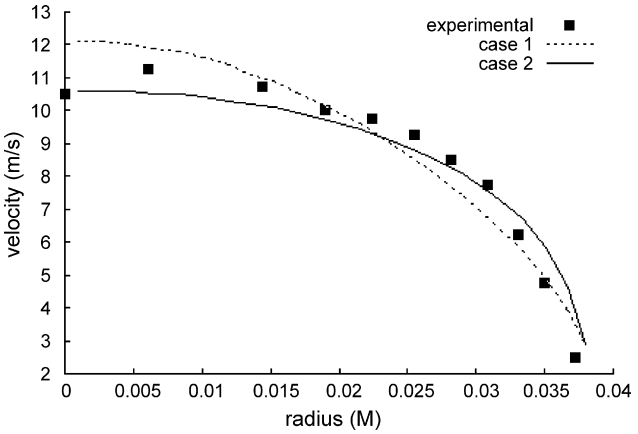

Fig. 10. Profiles of solids velocity at a height of 9.42 m.

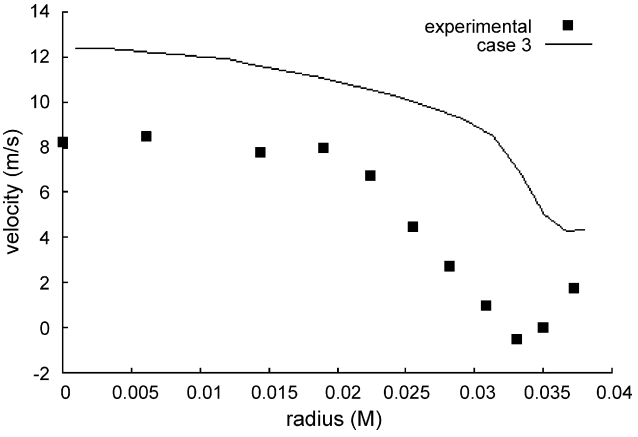

Fig. 11. Profiles of solids velocity at a height of 1.53 m.

entire zones by using the constant Newtonian coefficient (case 2) than the inviscid model (case 1). This becomes relevant in the region close to the wall. The results obtained with constant Newtonian coefficient follow the curve tendency satisfactorily.

Figs. 9 and 10 show profiles of velocity in the dilute region at heights of 8.74 m and 9.42 m, respectively. Both models showed great agreement with the experimental data. This shows that the dispersion model does not have a pronounced influence when solids concentration is low.

4.3. Radial profiles of the solids-phase velocity

The radial profiles of the solids-phase velocity were computed numerically at 37 s of real time, using a constant value for the solids-phase viscosity and the averaging procedure

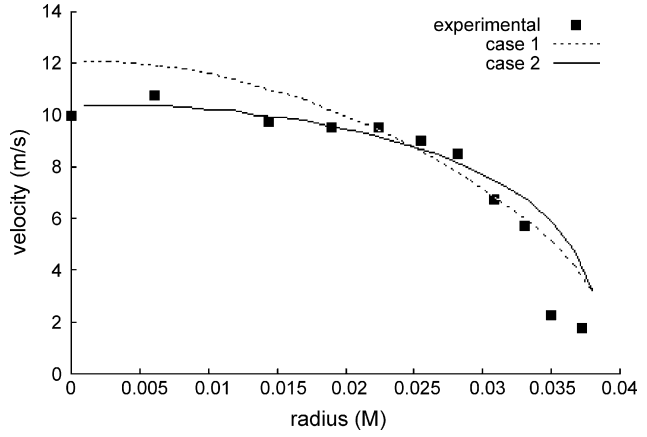

Fig. 9. Profiles of solids velocity at a height of 8.74 m.

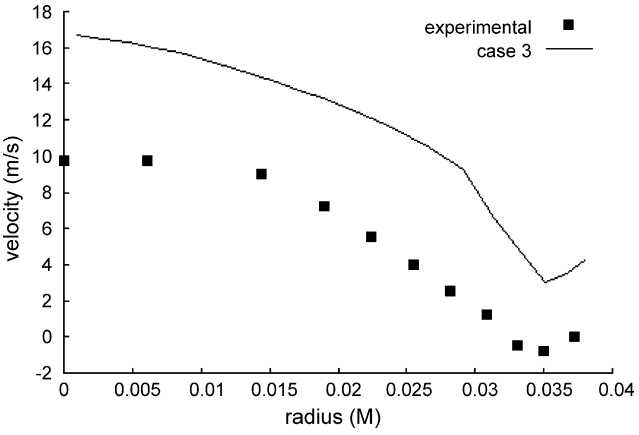

Fig. 12. Profiles of solids velocity at a height of 2.73 m.

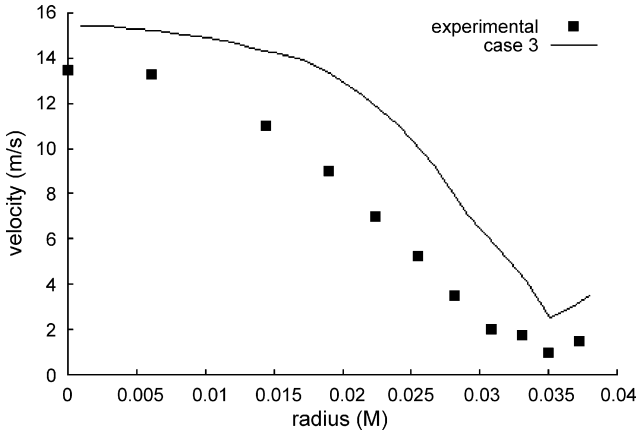

Fig. 13. Profiles of solids velocity at a height of 3.96 m.

at each iteration. This procedure showed good agreement between the volume fraction of the solids phase and the experimental data found in [18].

Figs. 11 and 12 show the dense region in the bottom section of the riser at heights of 1.53 m and 2.73 m, respectively. With the increase in computational time (case 3), one can see a better representation of the solids velocity profiles. Although the simulated results of case 3 somewhat overpredicted in the core and near the wall, one can see that the profiles in both figures show the tendency of the experimental data in the annulus region. The discrepancies between experimental and predicted results may be due to the fact that the solids-phase viscosity was considered constant. This parameter needs to be considered as a function of solids volume fraction in order to have a better representation of the radial profile of solids velocity.

Figs. 13–15 (at heights of 3.96 m, 5.13 m and 6.34 m, respectively) show the middle flow region. The results show good agreement in the core and annulus regions and a slight overprediction at a height of 6.34 m.

Figs. 16 and 17 (at heights of 8.74 m and 9.42 m, respectively) show the dilute region. The predicted radial solids velocities show good agreement with the measurements in both the core and annulus in the dilute region, except in the core regions for case 3 at a height of 8.74 m.

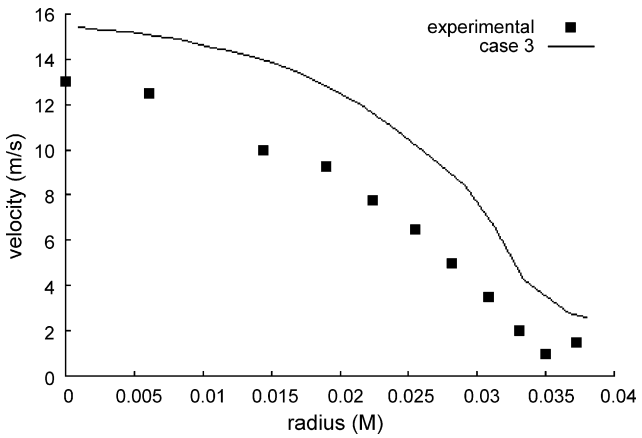

Fig. 14. Profiles of solids velocity at a height of 5.13 m.

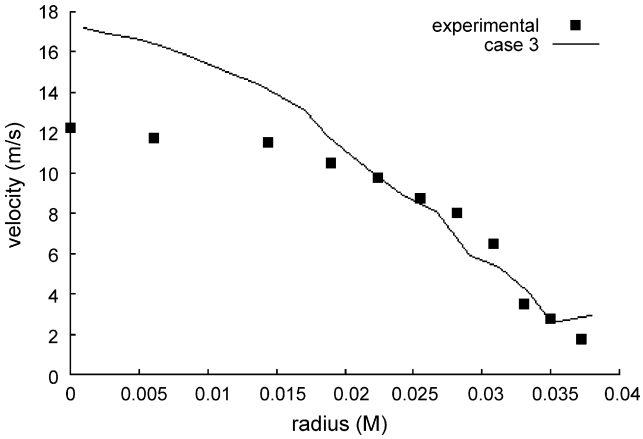

Fig. 15. Profiles of solids velocity at a height of 6.34 m.

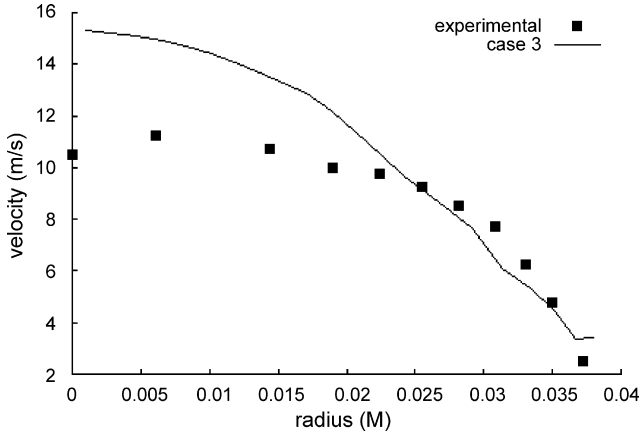

Fig. 16. Profiles of solids velocity at a height of 8.74 m.

In the wall region the particle velocity remains low until an approximate height of 6 m and increases slowly until reaching the dilute region at the top. Under a high solids flux, most of the particles are seen to flow upwards at the wall region. Under these conditions, the *core–annular* structure of the fast fluidization coexists with the ascending dense suspension. With the increase in solids flow at a constant superficial velocity

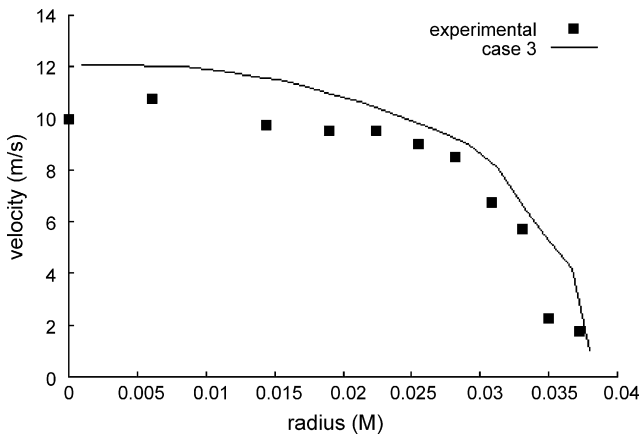

Fig. 17. Profiles of solids velocity at a height of 9.42 m.

of the gas phase, the upward flow of the dense suspension is in the dense region, while the fast fluidization is found in a higher. The velocity of the particulate solids phase is, in fact, higher in the central region than in the wall zone at all axial positions; along the riser axis, however, the velocity of the phase increases normally and slowly in the wall zone, reaching values greater than 10 m s^{-1} in the region of full flow, also in agreement with experimental data from [18].

5. Conclusions

Research dealing with high solids fluxes is required to improve and optimize the existing industrial HFCFBs. The k–ε gas-particle turbulence model is compared against experimental radial solids velocities on seven axial levels in a 76 mm ID and at a height of 10 m in a high-flux circulating fluidized bed (HFCFB) at a high flux of 300 kg m^{-2} s^{-1} and a superficial velocity of 8 m s^{-1}. The HFCFB riser is divided into three regions with a dense solids region in the bottom section (h = 0–4 m), a developed flow (h = 4–8 m) and a dilute region in the upper part (h = 8–10 m). The predicted radial solids velocities show good agreement with the measurements in both the core and annulus in the dilute region, except in the core regions for case 3 at a height of 8.74 m. The model predicts a core–annulus flow similar to that found experimentally in the middle flow region for cases 1–3, except at a height of 5.13 m, where a small deviation was seen. For all cases studied, the results overpredicted the velocity profiles in the dense region. The discrepancies between experimental and predicted results in the dense region may be due to the dependence of the effective viscosity on the solids volume fraction along the radial and axial directions.

Acknowledgements

The authors are grateful to PETROBRAS and to FAPESP for their financial support of this project.

References

[1] H. Ali, S. Rohani, Dynamic modelling and simulation of a riser-type fluid catalytic cracking unit, Chem. Eng. Technol. (20) (1997) 118–130.
[2] J.J.N. Alves, M. Mori, Fluid dynamic modelling and simulation of circulating fluidized bed reactors: analyses of particle phase stress models, Comput. Chem. Eng. 22 (1998) S763–S766.
[3] J.J.N. Alves, H.F. Meier, W.P. Martignoni, M. Mori, The effect of turbulence on the flow pattern of circulating fluidized bed reactors, in: Proceedings of ENPROMER, vol. 3, 2001, pp. 1351–1356.
[4] H. Arastoopour, C. Wang, A.W. Sanford, Particle–particle interaction force in a dilute gas–solid system, Chem. Eng. Sci. 37 (9) (1982) 1379–1386.
[5] C.T. Crowe, Review—numerical models for dilute gas–particle flows, J. Fluids Eng. 104 (1982) 297–303.
[6] C.T. Crowe, On models for turbulence modulation in fluid–particle flows, Int. J. Multiphase Flow (26) (2000) 719–727.
[7] D. Gidaspow, Multiphase Flow and Fluidization—Continuum and Kinetic Theory Descriptions, Academic Press, Inc., San Diego, CA, 1994.
[8] Y. He, V. Rudolph, Gas–solids flow in the riser of a circulating fluidized bed, Chem. Eng. Sci. 50 (21) (1995) 3443–3453.
[9] T.M. Knowlton, Experiment Modeling of Gas–Solid Flow System, Article Presented at CFDOIL-2005, Rio de Janeiro, 2005.
[10] D. Kunii, O. Levenspiel, Bubbling bed model for kinetic processes in fluidized beds, Ind. Eng. Chem. Process Des. Dev. 7 (4) (1968) 481–492.
[11] W.P. Martignoni, H.I. de Lasa, Heterogeneous reaction model for FCC riser units, Chem. Eng. Sci. 56 (2001) 605–612.
[12] H.F. Meier, M. Mori, The Eulerian–Eulerian–Lagragian model for cyclone simulation, in: Proceedings of the Fourth European Computational Fluid Dynamics Conference, vol. 1 (part 2), 1998, pp. 1206–1211.
[13] H.F. Meier, M. Mori, Anisotropic behavior of the reynolds stress in gas–solid flows in cyclones, Powder Technol. 101 (1999) 108–119.
[14] H.F. Meier, J.J.N. Alves, M. Mori, Comparison between staggered and collocated grids in the finite volume method performance for single and multiphase flows, Comput. Chem. Eng. 23 (1999) 247–262.
[15] E.E. Michaelides, A model for the flow of solid particles in gases, Int. J. Multiphase Flow 10 (1) (1984) 61–77.
[16] A. Neri, D. Gidaspow, Riser hydrodynamics: simulation using kinetic theory, AIChE J. 46 (1) (2000).
[17] J.J. Nieuwland, M.S. Annaland, J.A.M. Kuipers, W.P.M. Swaaij, Hydrodynamic modelling of gas/particle flows in riser reactors, AIChE J. 42 (6) (1996) 1569–1582.
[18] J.H. Pärssinen, J.X. Zhu, Axial and radial solids distribution in a long and high-flux CFB riser, AIChE J. 47 (10) (2001) 2197–2205.
[19] J.M. Rhodes, D. Geldart, A model for the circulating fluidized bed, Powder Technol. 53 (1987) 155–162.
[20] J.M. Rhodes, D. Geldart, The upward flow of gas/solid suspensions part i: a model for the circulating fluidized bed incorporating dual level gas entry into the riser, Chem. Eng. Res. Des. 67 (1989) 20–29.
[21] K. Rietema, H.E.A. van der Akker, On the momentum equations in dispersed two-phase system, Int. J. Multiphase Flow 9 (1) (1983) 21–36.
[22] A. Samuelsberg, B.H. Hjertager, Computational modelling of gas/particle flow in a riser, AIChE J. 42 (6) (1996) 1536–1546.
[23] S.L. Soo, Fluid Dynamics of Multiphase Systems, Blaisdell Publishing Co., Waltham, MA, 1967.
[24] K.N. Theologos, N.C. Markatos, Advanced modeling of fluid catalytic cracking riser-type reactors, AIChE J. 39 (6) (1993) 1007–1016.
[25] H. Yoshida, H. Masuda, Model simulation of particle motion in turbulent gas–solid pipe flow, Powder Technol. 26 (1980) 217–220.
[26] Y. Zhang, J.M. Reese, Gas turbulence modulation in a two-fluid model for gas–solid flows, AIChE J. 49 (12) (2003).